Improved SAR Imaging Via Cross-Learning from Camera Images

Improved SAR Imaging Via Cross-Learning from Camera Images

Shahzad Gishkori, David Wright, Liam Daniel, Marina Gashinova and Bernard Mulgrew

***Abstract*—In this paper, we propose a novel concept of cross-learning in order to improve synthetic aperture radar (SAR) images by learning from the camera images, in the manifold domain. We present multi-level abstraction approaches to materialise knowledge transfer between these two very different modalities (i.e., the radar and the camera), namely, a canonical correlation analysis (CCA) based approach and a manifold alignment based approach. We provide experimental results on real data, along with qualitative as well as quantitative analyses, to validate the proposed methodologies.**

***Index Terms*—SAR imaging, cross-learning, multi-modal fusion, manifold learning**

I. Introduction

Synthetic aperture radar (SAR) [1]–[3] can provide high-resolution images. Substantial amount of work is available to enhance SAR image quality in terms of denoising and/or super-resolution (see e.g., [4], [5] and references therein). SAR is emerging as a new imaging mode for automotive scenarios [6]–[8]. However, most of the previous work focuses on improving the SAR image by assuming SAR to be a stand-alone sensor, without any interaction with any sensor of a different modality. In automotive (especially, autonomous driving) scenarios, a car may be equipped with multiple sensors, e.g, radar, lidar, camera, etc [9], [10]. Therefore, it is natural to explore if a SAR image can be improved by using images from other sensors of different modalities, i.e., exploiting the framework of multi-modal fusion [11]–[13]. This motivation also forms the basis for our present paper.

Multi-modal fusion is a very generic concept, combining data/information from diverse modalities in order to enhance the achievement of a common objective, e.g., creating a unified sensing system, improving decision making, identifying/extracting specific features, etc. The key property is diversity, i.e., multiple modalities complementing each other in achieving a common goal in a way that cannot be achieved with a single modality [12]. Despite the unquestionable motivation for multi-modal fusion, the real challenge is how to exactly exploit this diversity. The reasons are that different modalities may be driven by different underlying variables or they may operate on different physical principles, etc. Therefore, finding a direct correspondence/correlation between them might not be straightforward. Some effort has been expended to devise a certain level of abstraction, e.g., [11], [14] (and references therein). However, more research needs to be done.

SAR and lidar are active sensor modalities. Some work on the fusion of hyperspectral SAR images and lidar images, in remote sensing domain, has appeared recently, e.g, in [15], [16]. A camera, in contrast, is a passive sensor modality and exploits illumination from other sources. Its ranging estimates (e.g., obtained by using the depth-maps for a stereo camera) are not as good as that of radar or lidar. However, it can provide very good image resolution. Due to the very different dynamics of SAR and camera sensors, e.g., operating principles, coordinate systems, pixel resolution, etc, it is quite hard to register and fuse their respective images. Generally, in the available work, e.g., [10], radar is primarily used as a detection sensor instead of an imaging sensor. Thus, according to our knowledge, not much work is available on the fusion of SAR and camera images.

In this paper, we focus on fusing SAR and camera images at the data level without (strictly) registering the respective images of the two sensors. To emulate automotive scenarios, we basically consider short-range radar sensing for extended targets (instead of point scatterers). Our primary aim is to reconstruct high-resolution SAR images, i.e, reconstructing the physical details of the extended target. In order to do this, we learn certain features of the target from camera images. Since these features have been learnt from a very different modality, we name this process as cross-learning. Note, cross-learning may have some overlap with transfer-learning [17]. However, the emphasis in the former is on different modalities. Cross-learning (from camera images) to improve SAR imaging is a very new concept and it has the potential to become a new area of research given the amount of challenges and opportunities associated with it. In this paper, we present approaches to materialise this concept. Our basic premise is the observation that despite difference in resolution and viewing perspective, both modalities try to capture the same physical geometry of the target. Therefore, correspondence or correlation between the two sensors does exist in some latent- or intrinsic-dimensional representation of their respective images. This may potentially circumvent the need for strict inter-sensor mapping/registration.

Traditionally, manifold learning techniques (linear or non-linear) [18]–[20] have been used to retrieve low-dimensional

S. Gishkori, D. Wright and B. Mulgrew are with Institute for Digital Communications (IDCOM), The School of Engineering, The University of Edinburgh, United Kingdom. Emails: {s.gishkori, bernie.mulgrew}@ed.ac.uk, dave_a_wright@yahoo.co.uk

L. Daniel and M. Gashinova are with Microwave Integrated System Laboratory (MISL), School of Electronic, Electrical and Systems Engineering, University of Birmingham, United Kingdom. Emails: {l.y.daniel, m.s.gashinova}@bham.ac.uk

This work was supported by Jaguar Land Rover and the UK-EPSRC grants EP/N012240/1 & EP/N012372/1 as part of the jointly funded Towards Autonomy: Smart and Connected Control (TASCC) Programme.

representation of a high-dimensional data for a wide range of tasks, e.g., detection, estimation, classification, visualisation, fusion, etc [21]–[25]. However, most of these tasks are (best) carried out in the manifold domain without the aim of reconstructing the high-dimensional data. In our case, we need to, *i)* create the respective manifolds of SAR and camera images to generate the intrinsic-dimensional or manifold-domain representation, *ii)* learn extra features from camera manifold and transfer it to the SAR manifold, *iii)* reconstruct the SAR image in its high-dimensional or image-domain representation. Since we do the learning in the manifold-domain and then reconstruct the original image-domain, we can only use linear manifolds, e.g, principal component analysis (PCA). Non-linear manifolds, e.g., Laplacian eigenmaps (LE), locally linear embedding (LLE), Hessian eigenmaps, diffusion maps etc, provide efficient low-dimensional representation. However, they cannot be transformed/projected back to the image domain. Manifold alignment (MFA) [24], [26], [27] has been an effective way of transferring knowledge/information between different datasets. Similarly, in the case of super-resolution of face images, building on a two step approach of global and then local features adjustment [28], [29], some authors, e.g., [30], [31] have advocated the creation of a coherent subspace over the manifolds for efficient transfer of knowledge. Due to an extra layer of abstraction, the latter approach has the ability to work with a modest amount of training samples as well as to compensate for choosing a linear manifold instead of a non-linear manifold (if required). Now, in case of transferring information from a camera image to a radar image, i.e., cross-learning, there are multiple challenges, e.g., the modalities are different, coordinate systems are different therefore the two sensors cannot be fully registered with each other, there is substantial disparity in resolution, choice of manifolds is limited due to reconstruction requirement, etc. Thus, in order to circumvent these challenges, a multi-level abstraction may be the right course of action. To this end, we follow the approach of [30]. We create PCA-based manifolds for both the sensors and generate a coherent subspace by using the canonical correlation analysis (CCA) [32], [33]. Then, we use LLE [21] to learn/adjust the neighbourhood embedding of the coherent subspace from the camera to the radar, followed by recovering the improved SAR image. Following the same logic, we also propose to extend the MFA approach of [27] by incorporating an LLE abstraction layer on the aligned PCA-based manifolds. Thus, rendering the MFA approach as a multi-level abstraction approach. Note, the input SAR images are generated by our recently proposed forward-scanning SAR (FS-SAR) [6] mode for the automotive scenarios, albeit, the synthetic aperture considered here is circular instead of linear, i.e., a circular-scanning SAR (CiS-SAR). Further, in this paper, we consider stationary targets, so that the presented work focuses on different aspects of the proposed method. However, future work will include scenarios with moving targets. In this regard, some of our recently published work in [7] may be useful in focusing the targets at a specific position to help in generating stable manifolds.

Contributions. The following are the main contributions of this paper.

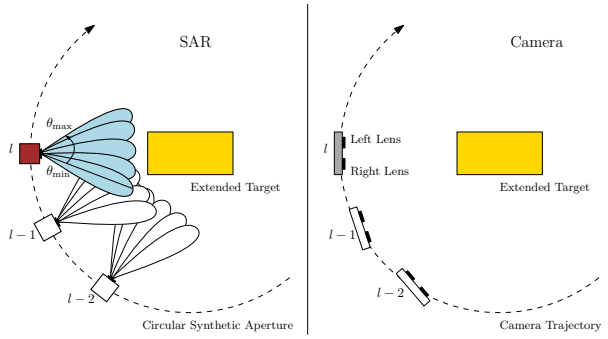

Fig. 1: SAR and Camera System Schematic

- We present a novel concept of improving SAR images via cross-learning from camera images.
- We show that multiple levels of abstraction can help circumvent the challenges of knowledge transfer in these different modalities.
- We consider a CiS-SAR mode generated SAR images as input to the cross-learning frame-work.
- We present performance results based on real-data obtained in our lab controlled experimental setup.

Advantages/Merits of the Proposed Method. The following are some of the expected advantages or merits of using our proposed method.

- Cross-learning helps in obtaining high-resolution SAR images which essentially helps in reconstructing the physical details of the extended targets. Thus, the resulting SAR images, having the benefit of both high-resolution as well as detailed information of the target, may possibly replace camera-only images for subsequent processing, e.g., segmentation, identification or classification.
- Through the use of manifolds, we are able to provide data level fusion between the SAR and camera images without strict registration, given that the two sensors share the same platform in viewing the same target. Thus, our approach is quite practical.
- Although we use CiS-SAR images as an example for short-range imaging, other SAR imaging methods can also be used in our cross-learning approach. Thus, our approach has the benefit of flexibility.

Organisation. Section II provides the system model, Section III elaborates on the realisation of cross-learning via different abstraction approaches, Section IV provides experimental results and performance comparisons, and Section V gives the conclusions.

Notations. Matrices are in upper case bold while column vectors are in lower case bold, $(\cdot)^T$ denotes transpose,$[\mathbf{a}]_i$ is the ith element of $\mathbf{a}$ and $[\mathbf{A}]_{i,j}$ is the ijth element of $\mathbf{A}$, $\hat{\mathbf{a}}$ is the estimate of $\mathbf{a}$, $\triangleq$ defines an entity, and the ℓ_p-norm is denoted as $||\mathbf{a}||_p = (\sum_{i=1}^{N} |[\mathbf{a}]_i|^p)^{1/p}$.

II. System Model

In [6], we proposed an FS-SAR mode to enhance the azimuth resolution of an automotive radar. This mode combines forward-scanning with SAR processing. FS-SAR assumes a

linear aperture. In the present paper, we consider a circular aperture, i.e., a circular-scanning SAR (CiS-SAR). CiS-SAR combines the benefits of scanning and spotlight SAR, resulting in enhanced azimuth resolution. We opt for CiS-SAR as a generic SAR mode in order to exhibit the cross-learning possibilities from camera to SAR. However, future works may consider other SAR modes as well. Figure 1 shows the schematic for CiS-SAR. At each scan-step, $l \in [1, L]$, over the circular aperture, the radar scans the extended target over the angular range (field of view of the sensor), $\theta \in [\theta_{\min}, \theta_{\max}]$. Thus, the target information is obtained both over the circular aperture as well as over the angular scan per aperture position. Similar to compressed sensing-based back-projection (CBP) in [6], we first process the measurements received over the scans by using a compressed sensing-based algorithm to improve the resolution and then back-project the reconstructed images from all the scans over the circular aperture to generate a coherent image of the extended target.

Let, the radar transmits frequency modulated continuous wave (FMCW) pulses towards the target. The signal received is then dechirped, low-pass filtered, deskewed, and Fourier transformed along the fast-time to obtain the range profile (see [6] for explicit expressions and subsequent details on the radar signal model). However, the received signal along the azimuth, for a scanning radar, at scan-step l and range r can be considered as a convolution of the radar antenna beam, $h(\theta)$, and the azimuth reflectivity function, $x_{l,r}(\theta)$, as in [34], i.e.,

$$y_{l,r}(\theta) = h(\theta) \star x_{l,r}(\theta) + \nu_{l,r}(\theta) \tag{1}$$

where $\star$ denotes convolution and $\nu_{l,r}(\theta)$ represents the additive white Gaussian noise (AWGN). Collecting all of the azimuth samples over θ, (1) can be written as

$$\mathbf{y}_{l,r} = \mathbf{G}\mathbf{H}\mathbf{x}_{l,r} + \boldsymbol{\nu}_{l,r} \tag{2}$$

where $\mathbf{H}$ is a block-Toeplitz convolution matrix and $\mathbf{G}$ is a selection matrix to balance the numeric relation between $N_x \times 1$ vector $\mathbf{x}_{l,r}$ and $N_\theta \times 1$ vector $\mathbf{y}_{l,r}$. Note, in the context of azimuth-resolution enhancement, $N_x \gg N_\theta$. Now, concatenating $\mathbf{y}_{l,r}$ over all N_r range bins, we can write (2) as

$$\mathbf{y}_l = \underbrace{[\mathbf{I}_{N_r} \otimes (\mathbf{G}\mathbf{H})]}_{\triangleq \mathbf{A}} \mathbf{x}_l + \boldsymbol{\nu}_l \tag{3}$$

where $\mathbf{y}_l \triangleq [\mathbf{y}_{l,1}^T, \mathbf{y}_{l,2}^T, \cdots, \mathbf{y}_{l,N_r}^T]^T$ is an $N_\theta N_r \times 1$ vector. Similarly, $\mathbf{x}_l$ and $\boldsymbol{\nu}_l$ can be defined as $N_x N_r \times 1$ and $N_\theta N_r \times 1$ vectors, respectively. Further, $\mathbf{A}$ is the $N_\theta N_r \times N_x N_r$ measurement matrix. Now, according to CBP, $\mathbf{x}_l$ (assuming it to be sparse) can be estimated by solving the following (fused LASSO [35]) optimisation problem.

$$\hat{\mathbf{x}}_l = \arg\min_{\mathbf{x}_l} \|\mathbf{y}_l - \mathbf{A}\mathbf{x}_l\|_2^2 + \lambda_e \|\mathbf{x}_l\|_1^1 + \lambda_f \|\mathbf{D}\mathbf{x}_l\|_1^1 \tag{4}$$

where λ_e and λ_f are positive penalty parameters controlling element-wise sparsity and fusion in $\mathbf{x}_l$, respectively, and $\mathbf{D}$ is the fusion matrix (i.e., $\mathbf{D}\mathbf{x}_l$ is a vector of differences of consecutive elements of $\mathbf{x}_l$) [35]. Then, the reconstructed radar image via back-projection, at pixel (i, j), can mathematically be represented as

$$\gamma_{i,j} = \sum_{l=1}^{L} [\uparrow_{1,\kappa'} (\hat{\mathbf{X}}_l)]_{I_{\theta_{i,j}}, I_{r_{i,j}}} \tag{5}$$

where $\uparrow_{\kappa,\kappa'} (\cdot)$ interpolates/upsamples a matrix by an order κ and κ' along its rows and columns, respectively, $\hat{\mathbf{X}}_l$ is the $N_x \times N_r$ reshaped matrix form of $\hat{\mathbf{x}}_l$, $[\cdot]_{I_{\theta_{i,j}}, I_{r_{i,j}}}$ represents the row and column indices of the matrix corresponding to angle $\theta_{i,j}$ and range $r_{i,j}$ for the (i, j)th pixel, respectively. Since each scanning position over the aperture may contribute to each pixel in the reconstructed image, we can rewrite (5) as

$$\gamma_{i,j} = \sum_{l=1}^{L} \gamma_{i,j}^l \tag{6}$$

where $\gamma_{i,j}^l \triangleq [\uparrow_{1,\kappa'} (\hat{\mathbf{X}}_l)]_{I_{\theta_{i,j}}, I_{r_{i,j}}}$. Let, all of the image pixels $\gamma_{i,j}^l$, for $i = 1, \cdots, \sqrt{N}$ and $j = 1, \cdots, \sqrt{N}$, w.r.t. contributions from the lth aperture position, are collected in an $N \times 1$ vector $\mathbf{r}_l$, i.e.,

$$\mathbf{r}_l \triangleq \left[\gamma_{1,1}^l, \cdots, \gamma_{\sqrt{N},1}^l, \gamma_{\sqrt{N},2}^l, \cdots, \gamma_{\sqrt{N},\sqrt{N}}^l\right]^T. \tag{7}$$

Now, we can collect all of the radar images generated from each aperture position, as defined in (7), as an $N \times L$ matrix $\mathbf{R}$, i.e.,

$$\mathbf{R} \triangleq [\mathbf{r}_1, \mathbf{r}_2, \cdots, \mathbf{r}_L]. \tag{8}$$

For the proposed cross-learning, we assume that the camera trajectory is the same as that of the radar synthetic aperture, i.e., the camera images of the target are also obtained from the same physical location as that of the radar. However, the camera does not involve any scanning and takes one snapshot for each location over its trajectory. Figure 1 shows the schematic of camera image acquisition. For the sake of clarity, the schematic for camera has been drawn separately from SAR. However, in practice, both sensors may share the physical location. The camera can be mono or stereo, with different image formats, i.e, RGB, greyscale, depth-map etc. It may also have its own requirements w.r.t. configuration, calibration, disparity/point-cloud formulation, etc. We assume that these pre-requisites have already been met. However, we do not assume any strict registration between the camera and the radar, as it is very difficult and our approach essentially tries to circumvent its need.

Let, a $\sqrt{M} \times \sqrt{M}$ generic camera image of the target at lth position on its trajectory is represented as an $M \times 1$ vector $\mathbf{s}_l$ via lexicographic ordering (column ordered). Then, we can collect all such images for the complete trajectory into an $M \times L$ matrix $\mathbf{S}$ as

$$\mathbf{S} \triangleq [\mathbf{s}_1, \mathbf{s}_2, \cdots, \mathbf{s}_L]. \tag{9}$$

The rest of the paper essentially deals with (8) and (9) in terms of proposing a cross-learning strategy.

III. Cross-Learning

In order to improve SAR images via cross-learning from camera images, we present two multi-level abstraction approaches, i.e., *i*) a multi-level CCA (ML-CCA) based cross-learning and *ii*) a multi-level MFA (ML-MFA) based cross-learning. For both the approaches, we first learn the respective manifolds of the training images of the two sensing modalities.

A. Suitable Manifold

As explained earlier, after cross-learning, we need to reconstruct the SAR image from low-dimensional space of the manifold domain to the high-dimensional space of the image domain. Therefore, non-linear manifolds cannot be used. In terms of linear manifolds, we opt for the classical PCA based manifolds.

PCA represents data by using the directions of maximum variance. Thus, it requires computing the principal eigenvectors of the data covariance matrix. Now, assuming that the datasets in (8) and (9) are centred (i.e., the corresponding sample means have been subtracted from them), the covariance matrices of radar and camera datasets can be defined as, $\mathbf{C}_r \triangleq (1/L)\mathbf{R}\mathbf{R}^T$ and $\mathbf{C}_s \triangleq (1/L)\mathbf{S}\mathbf{S}^T$, respectively. The eigenvalue decomposition (EVD) of the covariance matrices can then be carried out as

$$\text{EVD}(\mathbf{C}_r) = \mathbf{U}_r\mathbf{\Sigma}_r\mathbf{V}_r^T \tag{10}$$

$$\text{EVD}(\mathbf{C}_s) = \mathbf{U}_s\mathbf{\Sigma}_s\mathbf{V}_s^T \tag{11}$$

where matrices $\mathbf{U}_r$ and $\mathbf{U}_s$ contain the left eigenvectors, matrices $\mathbf{V}_r$ and $\mathbf{V}_s$ contain the right eigenvectors, and matrices $\mathbf{\Sigma}_r$ and $\mathbf{\Sigma}_s$ contain the corresponding eigenvalues along their diagonals, for radar and camera, respectively. The low-dimensional data representation essentially corresponds to projecting the data on a few significant eigenvectors. Let, n and m represent the number of significant eigenvectors (or subsequent principal components) for SAR and camera manifolds, respectively. Then, $\bar{\mathbf{U}}_r \triangleq [\mathbf{U}_r]_{:,1:n}$ and $\bar{\mathbf{U}}_s \triangleq [\mathbf{U}_s]_{:,1:m}$ are the $N \times n$ and $M \times m$ corresponding PCA-based projection matrices. The PCA-based projection coefficients can be obtained as

$$\mathbf{P}_r = \bar{\mathbf{U}}_r^T\mathbf{R} = [\mathbf{p}_{r_1}, \mathbf{p}_{r_2}, \cdots, \mathbf{p}_{r_L}] \tag{12}$$

$$\mathbf{P}_s = \bar{\mathbf{U}}_s^T\mathbf{S} = [\mathbf{p}_{s_1}, \mathbf{p}_{s_2}, \cdots, \mathbf{p}_{s_L}] \tag{13}$$

where $\mathbf{p}_{r_l} \triangleq \bar{\mathbf{U}}_r^T\mathbf{r}_l$, $\mathbf{p}_{s_l} \triangleq \bar{\mathbf{U}}_s^T\mathbf{s}_l$, and, $\mathbf{P}_r$ and $\mathbf{P}_s$ are $n \times L$ and $m \times L$ PCA coefficient matrices of SAR and camera manifolds, respectively.

B. ML-CCA Based Cross-learning

In ML-CCA based cross-learning, we first use CCA to generate a coherent subspace between the two modalities. Then, we use LLE for neighbourhood embedding w.r.t. test images of the radar and camera. Finally, the processed radar image is projected from the manifold domain back to the image domain.

1) Coherent Subspace: CCA finds a low-dimensional coherent subspace between two datasets. In this paper, we consider a one-dimensional CCA subspace. Thus, in our case, CCA provides one basis vector for each dataset such that the correlation between the corresponding projection coefficients is maximised. Note, the datasets, in our case, correspond to PCA-based manifold coefficients, i.e., (12) and (13). Mathematically, we can estimate the CCA-based subspace by solving the following optimisation problem, as in [32].

$$\left[\hat{\mathbf{b}}_r, \hat{\mathbf{b}}_s\right] = \underset{\mathbf{b}_r, \mathbf{b}_s}{\arg\max}\ \mathbf{b}_r^T\mathbf{Q}_{rs}\mathbf{b}_s \tag{14a}$$

$$\text{s.t. } \mathbf{b}_r^T\mathbf{Q}_r\mathbf{b}_r = 1,\ \mathbf{b}_s^T\mathbf{Q}_s\mathbf{b}_s = 1 \tag{14b}$$

where $\mathbf{b}_r$ and $\mathbf{b}_s$ are $n \times 1$ and $m \times 1$ canonical basis vectors for the radar- and camera-manifold datasets, respectively, and, $\mathbf{Q}_r \triangleq (1/L)\mathbf{P}_r\mathbf{P}_r^T$, $\mathbf{Q}_s \triangleq (1/L)\mathbf{P}_s\mathbf{P}_s^T$ and $\mathbf{Q}_{rs} \triangleq (1/L)\mathbf{P}_r\mathbf{P}_s^T$ are the corresponding covariance matrices. Note, the constraints (14b) are imposed to ensure a unique solution. Now, solving (14) essentially boils down to solving the following generalised eigenvalue problem (see [32] for details).

$$\begin{bmatrix} \mathbf{Q}_{rs}^T & \mathbf{0} \\ \mathbf{0} & \mathbf{Q}_{rs} \end{bmatrix} \begin{bmatrix} \mathbf{b}_r \\ \mathbf{b}_s \end{bmatrix} = 2\lambda \begin{bmatrix} \mathbf{0} & \mathbf{Q}_s \\ \mathbf{Q}_r & \mathbf{0} \end{bmatrix} \begin{bmatrix} \mathbf{b}_r \\ \mathbf{b}_s \end{bmatrix} \tag{15}$$

where λ is the generalised eigenvalue. Solving (14) is equivalent to finding the largest generalised eigenvalue in (15), i.e., $\lambda = \lambda_{\max}$, and the corresponding generalised eigenvector provides the estimate of canonical basis vectors as, $[\hat{\mathbf{b}}_r^T, \hat{\mathbf{b}}_s^T]^T$. From the basis vectors, the corresponding CCA-based coefficients can be obtained as

$$\mathbf{a}_r = \mathbf{P}_r^T\hat{\mathbf{b}}_r \tag{16}$$

$$\mathbf{a}_s = \mathbf{P}_s^T\hat{\mathbf{b}}_s \tag{17}$$

where $\mathbf{a}_r$ and $\mathbf{a}_s$ are $L \times 1$ vectors of CCA-based coefficients w.r.t. the radar and camera manifolds, respectively.

2) Neighbourhood Embedding: LLE is used to compute low-dimensional neighbourhood-preserving embeddings of high-dimensional data. It is based on a simple geometric intuition. Given a data point and its neighbours, in high-dimension, lie on a locally linear patch of the manifold, the data point can be reconstructed by linear combination of its neighbours. Then, the data point can be mapped to a low-dimensional representation while preserving its neighbourhood characterisation (see [21] for more details). In the context of cross-learning, *i)* the mapping is done from the camera manifold to the radar manifold, *ii)* the radar and the camera manifolds have been substituted with respective CCA-based coefficients which are linear due to one-dimensional CCA subspace and *iii)* in terms of CCA-based coefficients, the data dimension for both radar and camera is the same, therefore, we do not need to find the low-dimensional values. Thus, LLE can be easily applied to our case for neighbourhood embedding, i.e., we need to find the linear coefficients which reconstruct a camera data point from its neighbours and then use the same linear coefficients to reconstruct a radar data point from its neighbours. This constitutes neighbourhood embedding in the context of cross-learning.

Let, $\mathbf{r}_t$ and $\mathbf{s}_t$ be the test SAR and camera images, respectively, with $\mathbf{p}_{r_t} \triangleq \bar{\mathbf{U}}_r^T \mathbf{r}_t$ and $\mathbf{p}_{s_t} \triangleq \bar{\mathbf{U}}_s^T \mathbf{s}_t$ as the corresponding data points on the manifolds. Then, the CCA-based coefficients for the test images can be obtained as

$$a_{r_t} = \mathbf{p}_{r_t}^T \hat{\mathbf{b}}_r \tag{18}$$

$$a_{s_t} = \mathbf{p}_{s_t}^T \hat{\mathbf{b}}_s \tag{19}$$

where a_{r_t} and a_{s_t} are scalar values. Let, $\mathcal{N}_{r_t}^K$ and $\mathcal{N}_{s_t}^K$ represent the sets of K nearest neighbours (K-NN) of a_{r_t} and a_{s_t}, respectively. Now, we can write the optimisation problem of finding the linear coefficients of reconstructing a_{s_t} from its neighbours in $\mathbf{a}_s$ as a constrained least-squares fitting problem, i.e.,

$$\hat{\mathbf{w}} = \arg\min_{\mathbf{w}} \ \|a_{s_t} - \mathbf{w}^T \bar{\mathbf{a}}_s\|_2^2 \tag{20a}$$

$$\text{s.t.} \ \ \|\mathbf{w}\|_2^2 = 1 \tag{20b}$$

where $\bar{\mathbf{a}}_s$ is $K \times 1$ sub-vector of $\mathbf{a}_s$, such that, $[\mathbf{a}_s]_i \in \mathcal{N}_{s_t}^K$, for $i = 1, \cdots, K$. Note, (20) essentially applies two constraints, *i)* a sparseness constraint, i.e., weights are non-zero only for the K-NN of a_{s_t}, *ii)* an invariance constraint, i.e., the sum of linear coefficients equals one, as (20b). An efficient way to minimise the error in (20a) is to solve the following system of linear equations

$$\mathbf{G}\mathbf{w} = \mathbf{1} \tag{21}$$

where $\mathbf{G} \triangleq (a_{s_t} - \bar{\mathbf{a}}_s)(a_{s_t} - \bar{\mathbf{a}}_s)^T$, and then rescale the coefficients to satisfy (20b) (more details in [21]). Now, the learnt coefficients can be used to reconstruct the radar data point from the neighbours, i.e.,

$$\hat{a}_{r_t} = \hat{\mathbf{w}}^T \bar{\mathbf{a}}_r \tag{22}$$

where $\bar{\mathbf{a}}_r$ is $K \times 1$ sub-vector of $\mathbf{a}_r$, such that, $[\mathbf{a}_r]_i \in \mathcal{N}_{r_t}^K$, for $i = 1, \cdots, K$.

3) Image Reconstruction: After learning the CCA-based coefficient, the learnt radar image in the manifold domain can be obtained as

$$\tilde{\mathbf{p}}_{r_t} = (\hat{\mathbf{b}}_r^T)^\dagger \hat{a}_{r_t} + \mathbf{p}_{r_t} \tag{23}$$

where $(\cdot)^\dagger$ denotes the Moore-Penrose (or pseudo) inverse. Now, the radar image can be projected from the manifold domain back to the image domain as

$$\tilde{\mathbf{r}}_t = \bar{\mathbf{U}}_r \tilde{\mathbf{p}}_{r_t} \tag{24}$$

where $\tilde{\mathbf{r}}_t$ is the improved SAR image obtained via cross-learning from the camera image.

C. ML-MFA Based Cross-learning

In this section, we present ML-MFA based cross-learning. First, we reconstruct an image after manifold alignment (MFA) only, and then, we introduce the abstraction layer of neighbourhood embedding via LLE to distinguish between low-level abstraction and multi-level abstraction.

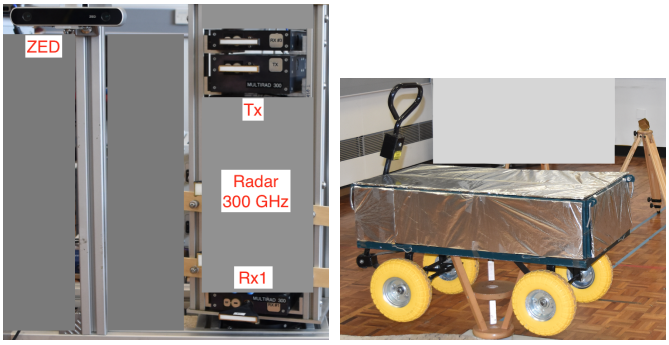

(a) ZED and Radar (300 GHz) (b) Trolley on a Turn-Table

Fig. 2: Experimental Setup

1) MFA: In this approach the PCA-based manifolds of the two sensors are essentially aligned using Procrustes analysis as in [27]. The basic idea is that given pairwise correspondence between the two datasets (assumed centred), a mapping is obtained to align the test data points. Using the earlier terminology developed in this paper, the following singular value decomposition (SVD) is performed as a first step.

$$\text{SVD}(\mathbf{P}_r \mathbf{P}_s^T) = \mathbf{U}\mathbf{\Sigma}\mathbf{V}^T \tag{25}$$

assuming $n = m$. Then, manifold alignment is obtained as

$$\hat{\mathbf{p}}_{r_t} = k\mathbf{Q}^T \mathbf{p}_{r_t} \tag{26}$$

where $k \triangleq \text{trace}(\mathbf{\Sigma})/\text{trace}(\mathbf{P}_r \mathbf{P}_r^T)$ and $\mathbf{Q} \triangleq \mathbf{U}\mathbf{V}^T$, and the MFA based SAR image can be obtained via (24) by using the relation, $\tilde{\mathbf{p}}_{r_t} = \hat{\mathbf{p}}_{r_t}$.

2) Neighbourhood Embedding: Now, we extend the MFA by neighbourhood embedding via LLE (similar to Section III-B2). This essentially forms the multi-level MFA (ML-MFA). Mathematically, it can be represented by re-writing (18) and (19) as

$$\mathbf{a}_{r_t} = \hat{\mathbf{p}}_{r_t}, \quad \mathbf{a}_{s_t} = \mathbf{p}_{s_t} \tag{27}$$

where $\mathbf{a}_{r_t}$ and $\mathbf{a}_{s_t}$ are vectors, and solving,

$$\hat{\mathbf{w}} = \arg\min_{\mathbf{w}} \ \|\mathbf{a}_{s_t} - \bar{\mathbf{A}}_s \mathbf{w}\|_2^2 \quad \text{s.t.} \ \|\mathbf{w}\|_2^2 = 1 \tag{28}$$

where $\bar{\mathbf{A}}_s$ is a matrix containing K neighbours of $\mathbf{a}_{s_t}$ in $\mathbf{P}_s$, as its columns, and re-writing (22) as

$$\hat{\mathbf{a}}_{r_t} = \bar{\mathbf{A}}_r \hat{\mathbf{w}} \tag{29}$$

where $\bar{\mathbf{A}}_r$ is a matrix containing K neighbours of $\mathbf{a}_{r_t}$ in $k\mathbf{Q}^T\mathbf{P}_r$, as its columns. Then, by using the relation $\tilde{\mathbf{p}}_{r_t} = \hat{\mathbf{a}}_{r_t}$, SAR image can be obtained via (24).

IV. Experimental Results

In this section, we validate the proposed concept of cross-learning between SAR and camera images by experimental results. According to our knowledge, a public dataset for concurrent SAR and camera measurements is not available. Therefore, as part of this research, we have carried out such

TABLE I: Specifications of 300 GHz Radar

Modulation	FMCW
Frequency Range	$287 - 293$ GHz
Transmit Bandwidth (B)	5 GHz
Chirp Duration (T)	1 ms
Sampling Frequency	4.096 MHz
Angular Step (Δ_θ)	0.25°
Range Resolution (Δ_r)	0.03 m
Two-way 3 dB Beamwidth ($\theta_{3\text{dB}}$)	1.3°

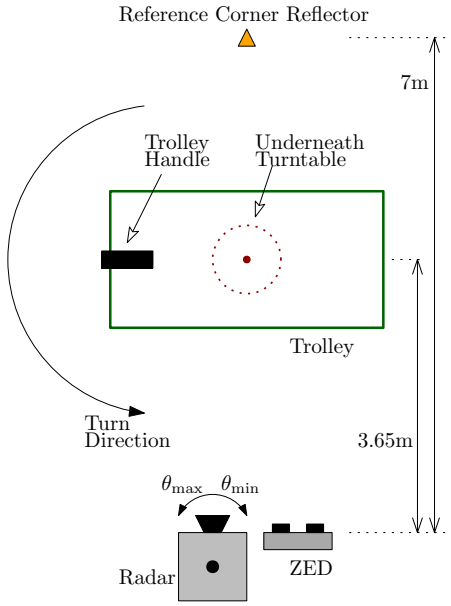

Fig. 3: Measurement Schematic

measurements in a laboratory controlled environment[1]. Our experimental setup (see Figure 2) mainly consists of a ZED stereo camera (see [36] for specifications), a 300 GHz FMCW radar (see Table I for specifications) and a trolley (of size $1 \times 0.5 \times 0.55$ (length $\times$ width $\times$ height) m^3) on a turntable. Figure 3 shows the measurement schematic of the experiment. The trolley is placed on a turntable at a distance of 3.65 m from the joint sensors (ZED and radar) platform. Measurements from the sensors are taken for every 5 degree angular turn (counter clock-wise) of the trolley. This emulates the circular motion of the sensors around the target. Thus, $L = 72$ (synthetic) aperture samples are obtained all around the trolley. Note, in this paper, we consider a full 360° circular aperture for the purpose of illustration only. However, in practice, the target can be seen by a partial aperture. For every aperture sample, we consider only left lens RGB image from the ZED. We convert the RGB image to a greyscale image. Figure 4 shows the ZED images of the trolley at different positions (on the truntable) $l = 1\,(0^\circ), 19\,(90^\circ), 37\,(180^\circ), 55\,(270^\circ)$. At every aperture position, the radar scans the target scene for an angular range $\theta = \pm 13^\circ$, at angular intervals $\Delta_\theta = 0.25^\circ$. Then, using (4) and (7), a SAR image is created for every lth

[1]All real-data supporting this work are openly available from The University of Edinburgh repository (DataShare) at https://doi.org/10.7488/ds/2828

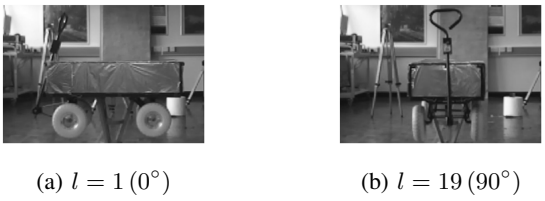

(a) $l = 1\,(0^\circ)$ (b) $l = 19\,(90^\circ)$

(c) $l = 37\,(180^\circ)$ (d) $l = 55\,(270^\circ)$

Fig. 4: ZED Greyscale Images

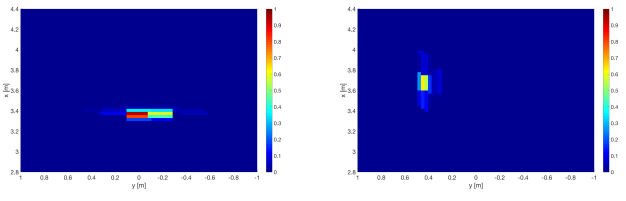

(a) $l = 1\,(0^\circ)$ (b) $l = 19\,(90^\circ)$

(c) $l = 37\,(180^\circ)$ (d) $l = 55\,(270^\circ)$

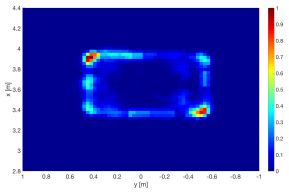

(e) CiS-SAR

Fig. 5: SAR Images

aperture position. Finally, a combined image of the target is achieved by using (5). Figure 5 shows the SAR images for $l = 1\,(0^\circ), 19\,(90^\circ), 37\,(180^\circ), 55\,(270^\circ)$ and the combined CiS-SAR image of the trolley. Note, all SAR images have been normalised so that the maximum intensity is unity. We can see that the SAR images of individual apertures, Figures 5a–5d, capture viewing-angle dependent information of the target. Nonetheless, the combined image, Figure 5e, provides very good imaging result in capturing the complete outline of the target, which re-affirms the enhanced performance of CBP reconstruction algorithm as proposed in [6]. However, we can see that the handle of the trolley is not very prominent.

Now, in order to improve SAR imaging results we use the cross-learning concept as explained in Section III. Using (12) and (13), for $n = m = 15$ principal components, we obtain the PCA based manifolds of the images of the two

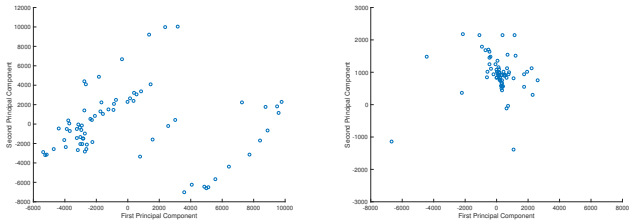

(a) Camera Manifold (b) SAR Manifold

Fig. 6: PCA-based Manifolds

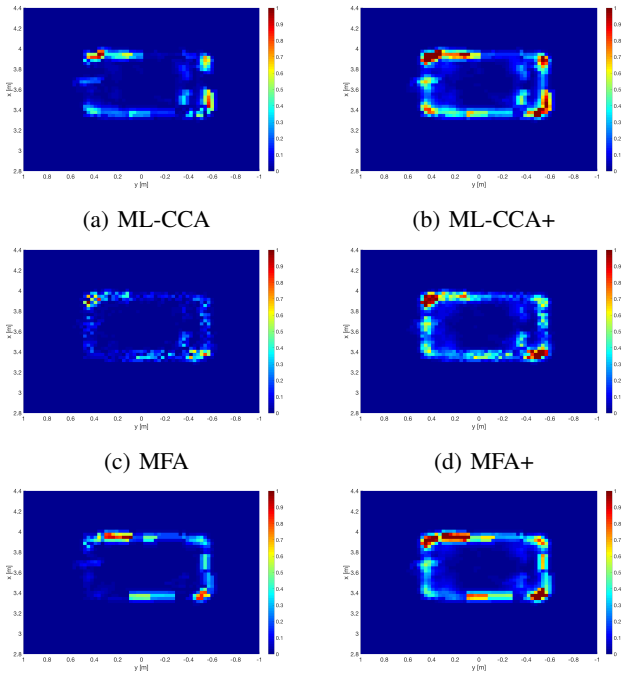

(a) ML-CCA (b) ML-CCA+

(c) MFA (d) MFA+

(e) ML-MFA (f) ML-MFA+

Fig. 7: Cross-Learning

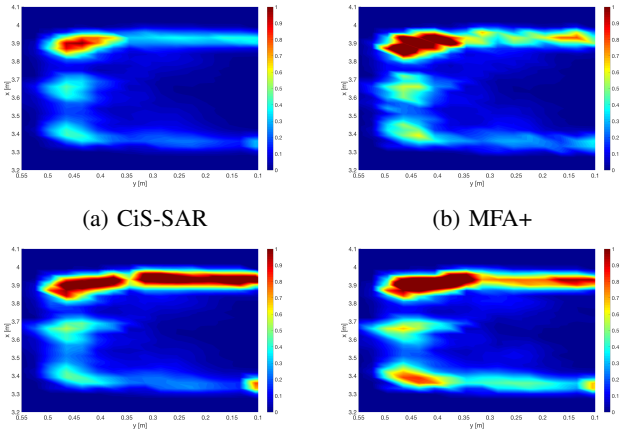

(a) CiS-SAR (b) MFA+

(c) ML-MFA+ (d) ML-CCA+

Fig. 8: Comparison of different methods

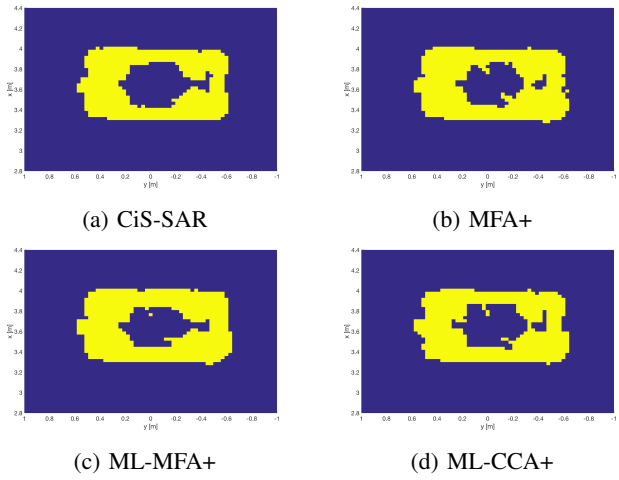

(a) CiS-SAR (b) MFA+

(c) ML-MFA+ (d) ML-CCA+

Fig. 9: Pseudo-ground-truths

sensors. Note, we chose these number of principal components as they seemed to provide good results from a qualitative perspective. However, given the training data, a better estimate can easily be found. Nonetheless, in our experience, changing these numbers does not have a drastic impact on the trend of performance, as would become clear shortly. Figure 6 shows these manifolds (as scatter plots) for first two principal components. We can see that the ZED manifold is more elaborate than the SAR manifold (which is quite concentrated). This shows that the ZED images are more distinguishable than the SAR images. Thus, the SAR images have a big margin of learning from the camera images.

Figure 7a shows the SAR image using ML-CCA approach. Note, we essentially use all of the training images as the test images, i.e., $t = 1, \cdots, L$, for both the sensors. We can see that in comparison to CiS-SAR (Figure 5e), ML-CCA image has captured some new information of the target. The walls of the trolley are more prominent. However, the most interesting aspect is the visibility of the trolley handle. Nonetheless, we can see that the target information both in CiS-SAR and ML-CCA does not seem to overlap for every pixel. Thus, a natural course of action is to combine the two images. We name the combined CiS-SAR and ML-CCA image as ML-CCA+. Figure 7b shows the ML-CCA+ image. We can see that it is a much improved image than the CiS-SAR as in Figure 5e.

Figure 7c shows the imaging result of MFA approach (which uses low-level of abstraction). Similar to ML-CCA+, we also provide the image result of MFA+ in Figure 7d. We can see that MFA does get some extra information in comparison to CiS-SAR (Figure 5e). However, its performance is inferior to ML-CCA (Figure 7a). Similarly, ML-CCA+ (Figure 7b) provides better result than MFA+.

Figure 7e shows the imaging result of ML-MFA. Similar to ML-CCA+, we also provide the image result of ML-MFA+ in Figure 7f. We can see that ML-MFA is also showing some features of the trolley handle. Therefore, ML-MFA+ shows an improved image. It is better than MFA+ (Figure 7d), since it uses multi-level abstraction.

Figure 8 provides images, zoomed in on the trolley front-end, created by CiS-SAR, MFA+, ML-MFA+ and ML-CCA+, to better assess the qualitative comparison. Note, we have also used Matlab's smoothing function to reduce pixelation (for

TABLE II: Comparison ($n = m = 15$)

	CiS-SAR	ML-CCA+	MFA+	ML-MFA+
CiS-SAR	0.9259	0.9234	0.9150	0.9141
ML-CCA+	0.9327	0.9292	0.9210	0.9196
MFA+	0.9303	0.9272	0.9190	0.9179
ML-MFA+	0.9348	0.9310	0.9220	0.9201

TABLE III: Comparison ($n = m = 5$)

	CiS-SAR	ML-CCA+	MFA+	ML-MFA+
CiS-SAR	0.9259	0.9274	0.9237	0.9170
ML-CCA+	0.9293	0.9308	0.9265	0.9201
MFA+	0.9290	0.9308	0.9262	0.9196
ML-MFA+	0.9305	0.9325	0.9274	0.9207

better display). We can see that cross-learning has helped in collecting more information of the target. In particular, ML-MFA+ and ML-CCA+ which use multi-level abstraction, show more reflectivity and structure of the trolley (i.e., walls and handle) than CiS-SAR.

Now, in order to provide quantitative analyses of the presented methods, we need a ground truth which is not easy to obtain. To circumvent this, we consider a pseudo-ground-truth. We estimate the noise level in the generated image of each method via a histogram (i.e., the most populated bin in a histogram of 50 bins) and remove it from the respective image. Then, we quantify all reflectivity values to unity. This provides us a pseudo-ground-truth, albeit favouring its generative method. Figure 9 shows the resulting images. We can see that with small variations, all the images look quite similar. Thus, these can serve as approximate ground truths for all the methods. We basically take each of these images and then compare the performance of all methods with it. For quantitative comparison, we use Matlab's function `ssim` which is a structural similarity index metric for image comparison, i.e., it combines local image structure, luminance, and contrast into a single local quality score. In our case, it would basically measure the structure and total reflectivity of each image in comparison to the ground truth. Note, 1 is the highest `ssim` score. Table II provides the comparison results. The column represent the ground truth image used and the rows provide the similarity measure for each method. We can see that for all the cases, multi-level abstraction based methods, i.e., ML-MFA+ and ML-CCA+, perform much better than the others. MFA+ basically uses low-level of abstraction, but still outperforms CiS-SAR. Table II provides the comparison results for the PCA order $n = m = 15$. We also present results by varying PCA order to $n = m = 5$ and $n = m = 25$, in order to see the impact of such variations, in Tables III and IV, respectively. We can see that there is not much difference in the general trend of performance. However, given the training data, an appropriate value of PCA order can always be found. From above, we can say that multi-level abstraction approaches have superior performance in realising the concept of cross-learning to improve SAR images by using the camera images.

TABLE IV: Comparison ($n = m = 25$)

	CiS-SAR	ML-CCA+	MFA+	ML-MFA+
CiS-SAR	0.9259	0.9234	0.9153	0.9134
ML-CCA+	0.9295	0.9270	0.9186	0.9163
MFA+	0.9271	0.9245	0.9172	0.9150
ML-MFA+	0.9344	0.9313	0.9229	0.9192

V. Conclusions

In this paper, we have proposed a novel concept of cross-learning, in order to improve SAR images by learning from the camera images. Despite the fact that the two sensors are very different modalities, we have used multi-level abstraction approaches to achieve knowledge transfer between them. To this end, we have presented a CCA based multi-level abstraction approach and a manifold alignment based multi-level abstraction approach. In order to validate the proposed concept, we have provided experimental results on real data. Through qualitative and quantitative analyses, we have shown that multi-level abstraction approaches provide better performance results in terms of collecting more information about the target structure.

References

[1] W. Carrara, R. Goodman, and R. Majewski, *Spotlight Synthetic Aperture Radar*. Boston: Artech House, 1995.

[2] C. Jakowatz, D. Wahl, P. Eichel, D. Ghiglia, and P. Thompson, *Spotlight-Mode Synthetic Aperture Radar: A Signal Processing Approach*. MA, USA: Kulwer Academic Publishers, 1996.

[3] M. Soumekh, *Synthetic Aperture Radar Signal Processing with MATLAB Algorithms*. NY, USA: John Wiley & Sons, Inc., 1999.

[4] M. Cetin, I. Stojanovic, O. Onhon, K. Varshney, S. Samadi, W. C. Karl, and A. S. Willsky, "Sparsity-driven synthetic aperture radar imaging: Reconstruction, autofocusing, moving targets, and compressed sensing," *IEEE Signal Processing Magazine*, vol. 31, no. 4, pp. 27–40, July 2014.

[5] S. Gishkori and B. Mulgrew, "Graph signal processing-based imaging for synthetic aperture radar," *IEEE Geoscience and Remote Sensing Letters*, p. to appear, 2019.

[6] S. Gishkori, L. Daniel, M. Gashinova, and B. Mulgrew, "Imaging for a forward scanning automotive synthetic aperture radar," *IEEE Transactions on Aerospace and Electronic Systems*, vol. 55, no. 3, pp. 1420–1434, June 2019.

[7] S. Gishkori, D. Wright, L. Daniel, M. Gashinova, and B. Mulgrew, "Imaging moving targets for a forward-scanning automotive SAR," *IEEE Transactions on Aerospace and Electronic Systems*, vol. 56, no. 2, pp. 1106–1119, 2020.

[8] I. Bilik, O. Longman, S. Villeval, and J. Tabrikian, "The rise of radar for autonomous vehicles: Signal processing solutions and future research directions," *IEEE Signal Processing Magazine*, vol. 36, no. 5, pp. 20–31, Sep. 2019.

[9] E. Guizzo, "How Google's self-driving car works," Oct. 2011. [Online]. Available: https://spectrum.ieee.org/automaton/robotics/artificial-intelligence/how-google-self-driving-car-works

[10] H. Cho, Y. Seo, B. V. K. V. Kumar, and R. R. Rajkumar, "A multi-sensor fusion system for moving object detection and tracking in urban driving environments," in *2014 IEEE International Conference on Robotics and Automation (ICRA)*, May 2014, pp. 1836–1843.

[11] B. Khaleghi, A. Khamis, F. O. Karray, and S. N. Razavi, "Multisensor data fusion: A review of the state-of-the-art," *Inf. Fusion*, vol. 14, no. 1, pp. 28–44, Jan. 2013.

[12] D. Lahat, T. Adali, and C. Jutten, "Multimodal data fusion: An overview of methods, challenges, and prospects," *Proceedings of the IEEE*, vol. 103, no. 9, pp. 1449–1477, Sep. 2015.

[13] D. Ramachandram and G. W. Taylor, "Deep multimodal learning: A survey on recent advances and trends," *IEEE Signal Processing Magazine*, vol. 34, no. 6, pp. 96–108, Nov 2017.

[14] L. Sorber, M. Van Barel, and L. De Lathauwer, "Structured data fusion," *IEEE Journal of Selected Topics in Signal Processing*, vol. 9, no. 4, pp. 586–600, June 2015.

[15] C. Debes, A. Merentitis, R. Heremans, J. Hahn, N. Frangiadakis, T. van Kasteren, W. Liao, R. Bellens, A. Pizurica, S. Gautama, W. Philips, S. Prasad, Q. Du, and F. Pacifici, "Hyperspectral and LiDAR data fusion: Outcome of the 2013 GRSS data fusion contest," *IEEE Journal of Selected Topics in Applied Earth Observations and Remote Sensing*, vol. 7, no. 6, pp. 2405–2418, June 2014.

[16] M. Dalla Mura, S. Prasad, F. Pacifici, P. Gamba, J. Chanussot, and J. A. Benediktsson, "Challenges and opportunities of multimodality and data fusion in remote sensing," *Proceedings of the IEEE*, vol. 103, no. 9, pp. 1585–1601, Sep. 2015.

[17] S. J. Pan and Q. Yang, "A survey on transfer learning," *IEEE Transactions on Knowledge and Data Engineering*, vol. 22, no. 10, pp. 1345–1359, Oct 2010.

[18] C. M. Bishop, *Pattern Recognition and Machine Learning (Information Science and Statistics)*. Berlin, Heidelberg: Springer-Verlag, 2006.

[19] X. Huo and A. Smith, "A survey of manifold-based learning methods," *Recent Advances in Data Mining of Enterprise Data*, pp. 691–745, 2008.

[20] L. van der Maaten, E. Postma, and J. van den Herik, "Dimensionality reduction: A comparative review," Tilburg University, Tech. Rep., Oct. 2009.

[21] S. T. Roweis and L. K. Saul, "Nonlinear dimensionality reduction by locally linear embedding," *Science*, vol. 290, pp. 2323–2326, 2000.

[22] M. Belkin and P. Niyogi, "Laplacian eigenmaps for dimensionality reduction and data representation," *Neural Comput.*, vol. 15, no. 6, pp. 1373–1396, Jun. 2003.

[23] M. B. Wakin, D. L. Donoho, H. Choi, and R. G. Baraniuk, "The multiscale structure of non-differentiable image manifolds," in *SPIE Conference Series*, 2005, pp. 413–429.

[24] S. Lafon, Y. Keller, and R. R. Coifman, "Data fusion and multicue data matching by diffusion maps," *IEEE Trans. Pattern Anal. Mach. Intell.*, vol. 28, no. 11, pp. 1784–1797, Nov. 2006.

[25] M. A. Davenport, C. Hegde, M. F. Duarte, and R. G. Baraniuk, "Joint manifolds for data fusion," *IEEE Transactions on Image Processing*, vol. 19, no. 10, pp. 2580–2594, Oct 2010.

[26] J. Ham, D. Lee, and S. Lawrence, "Semisupervised alignment of manifolds," *Proceedings of the Annual Conference on Uncertainty in Artificial Intelligence*, vol. 10, pp. 120–127, Jan 2005.

[27] C. Wang and S. Mahadevan, "Manifold alignment using procrustes analysis," in *Proceedings of the 25th International Conference on Machine Learning*, 2008, pp. 1120–1127.

[28] C. Liu, H.-Y. Shum, and W. T. Freeman, "Face hallucination: Theory and practice," *International Journal of Computer Vision*, vol. 75, no. 1, pp. 115–134, Oct 2007.

[29] Hong Chang, Dit-Yan Yeung, and Yimin Xiong, "Super-resolution through neighbor embedding," in *Proceedings of the 2004 IEEE Computer Society Conference on Computer Vision and Pattern Recognition, 2004. CVPR 2004.*, vol. 1, June 2004, pp. I–I.

[30] H. Huang, H. He, X. Fan, and J. Zhang, "Super-resolution of human face image using canonical correlation analysis," *Pattern Recogn.*, vol. 43, no. 7, pp. 2532–2543, Jul. 2010.

[31] H. Huang and H. He, "Super-resolution method for face recognition using nonlinear mappings on coherent features," *IEEE Transactions on Neural Networks*, vol. 22, no. 1, pp. 121–130, Jan 2011.

[32] D. R. Hardoon, S. Szedmak, and J. Shawe-Taylor, "Canonical correlation analysis: An overview with application to learning methods," *Neural Computation*, vol. 16, no. 12, pp. 2639–2664, 2004.

[33] A. J. Izenman, *Modern Multivariate Statistical Techniques: Regression, Classification, and Manifold Learning*, 1st ed. Springer Publishing Company, Incorporated, 2008.

[34] M. A. Richards, *Fundamentals of Radar Signal Processing*. Two Penn Plaza, NY, USA: McGraw-Hill Companies, Inc., 2005.

[35] R. Tibshirani, M. Saunders, S. Rosset, J. Zhu, and K. Knight, "Sparsity and smoothness via the fused LASSO," *Journal of the Royal Statistical Society Series B*, pp. 91–108, 2005.

[36] "ZED stereo camera," https://www.stereolabs.com/.

Shahzad Gishkori received the B.Sc. degree in electrical engineering from the University of Engineering and Technology Lahore, Lahore, Pakistan, in 2002, and the M.Sc. (cum Laude) and Ph.D. degrees both in electrical engineering from the Delft University of Technology, Delft, The Netherlands, in 2009 and 2014, respectively.
From 2014 to 2015, he was a Postdoctoral Research Associate with Imperial College London, London, U.K. From 2016 to 2020, he was a Postdoctoral Research Associate with the University of Edinburgh, Edinburgh, U.K, and currently is a visiting researcher there. His research interests include compressed sensing, signal processing for wireless communications and image processing for automotive radars.

David Wright received a BSc. in Geophysics in 1998 from the University of Edinburgh, MSc. in applied Geophysics from the University of Durham in 1999 and PhD. in exploration Geophysics from the University of Edinburgh in 2004.
He was co-founder and senior geophysicist at MTEM Ltd. from 2004–2007 and senior research geophysicist at Petroleum Geo Services from 2007–2010. From 2010–2016 he was a research fellow in the School of Geosciences at the University of Edinburgh. From 2018–2019 he was a research associate at the institute of digital communications at the University of Edinburgh working on radar imaging for autonomous vehicles.

Liam Daniel received the M.Sc. degree in theoretical physics in 2005 and the Ph.D. degree in maritime forward scatter radar development in 2017, both from the University of Birmingham, Birmingham, U.K.
He is currently a Research Fellow at the Microwave Integrated Systems Laboratory, School of Engineering, University of Birmingham, Birmingham, U.K. His research interests include experimental, theoretical, simulation and signal processing aspects of bistatic radars with a focus on forward scatter radar and passive sensing, automotive sensing, and low-THz radar systems.

Marina Gashinova received the M.Math degree from St.-Petersburg State University, Saint Petersburg, Russia, in 1991, and the Ph.D. degree in physics and mathematics from St.-Petersburg Electrotechnical University, Saint Petersburg, Russia, in 2003.
In 2006, she joined the Microwave Integrated System Laboratory, University of Birmingham, Birmingham, U.K., as a Research Fellow. She is currently a Professor of Radar and RF Sensors, leading the research group on passive and active bistatic radar, THz multi-feature imaging radar, and automotive sensors.

Bernard Mulgrew (FIEEE, FREng, FRSE, FIET) received the B.Sc. degree from Queen's University Belfast, Belfast, U.K., in 1979, and the Ph.D. degree from University of Edinburgh, Edinburgh, U.K., in 1987.

After graduation, he worked for 4 years as a Development Engineer with the Radar Systems Department, Ferranti, Edinburgh. From 1983 to 1986, he was a Research Associate with the Department of Electrical Engineering, University of Edinburgh, Edinburgh, U.K. He was appointed as a Lecturer in 1986, promoted to a Senior Lecturer in 1994 and became a Reader in 1996. The University of Edinburgh appointed him to a Personal Chair in October 1999 (Professor of Signals and Systems). He has co-authored three books on signal processing. His research interests include adaptive signal processing and estimation theory and in their application to radar and sensor systems.